



# Coupling Dependence on Chaos Synchronization Process in a Network of Rulkov Neurons

Gabriel Marghoti

*Universidade Federal do Paraná, Physics Department,  
Curitiba, Paraná 81531-980, Brazil  
gabrielmarghoti@gmail.com*

Fabiano Alan Serafim Ferrari

*Departamento de Física, Universidade Tecnológica Federal do Paraná,  
Pato Branco-PR, Brazil*

*Programa de Pós-Graduação em Modelagem Computacional e Sistemas,  
Universidade Estadual de Montes Claros, Montes Claros-MG, Brazil*

Ricardo Luiz Viana, Sergio Roberto Lopes and Thiago de Lima Prado  
*Universidade Federal do Paraná, Physics Department,  
Curitiba, Paraná 81531-980, Brazil*

Received May 12, 2023; Revised August 11, 2023

This paper investigates the impact of network conformation on chaos synchronization in driven complex networks in a master-slave setting. We analyze the control and prediction of complex networks under perturbations. Although chaotic dynamics suppression is well understood in low-dimensional systems, it is not well described in more complex ones. To assess a network's ability to amplify or suppress disturbances, we track ensembles of possible trajectories in the driven subsystem which give insights into nonlocal convergence properties in a master-slave setting. We demonstrate how the stability of forced networks of Rulkov neurons is dependent on network coupling architecture and how the duration of chaotic transients depends on initial conditions. Furthermore, we find that each network generator algorithm has specific sets of parameters that can lead to stable or nonstable states. Our results indicate that network types are more critical than isolated connections for suppressing chaotic dynamics in driven networks. Finally, we identify that under certain circumstances, the transient period before synchronization correlates with high convergence rates for certain initial conditions. This suggests nonuniform convergence rates in the phase space of driven neural networks.

**Keywords:** Chaos synchronization; complex network; conditional Lyapunov exponents; driven system; Rulkov map.

## 1. Introduction

Several studies have reported the synchronization of low-dimensional chaotic systems forced by a driver [Pecora & Carroll, 1990; Boccaletti *et al.*, 2002; Eroglu *et al.*, 2017]. However, chaos synchronization in complex neuronal networks, which have a large number of parameters and degrees of freedom, is not well understood.

In this work, we investigate how connection architecture affects chaos synchronization in a network of chaotic oscillators. When a nonlinear chaotic subsystem is forced by a common signal, it may exhibit similar trajectories regardless of initial conditions, known as chaos synchronization (CS) [Pecora & Carroll, 1990], or also known as complete synchronization when the trajectories are identical

[Boccaletti *et al.*, 2002]. We use the master-slave configuration, where one subsystem forces another without reciprocity [Lerescu *et al.*, 2004]. However, CS is not limited to master-slave systems, and other coupling configurations that incorporate some driver feature may enable the phenomenon, such as variable driving other than found in the same system [Eroglu *et al.*, 2017; Pecora & Carroll, 1990], or the addition of external noise [Maritan & Banavar, 1994].

Additionally, it has been shown that chaos can be controlled by the addition of random signals, similar to noise. For example, two Lorenz systems can undergo the same trajectory when forced by the same noise signal [Maritan & Banavar, 1994].

Chaos synchronization (CS) is a well-known phenomenon in low-dimensional systems, and its quantification is commonly achieved by conditional Lyapunov exponents (CLE) [Pecora & Carroll, 1991; Soriano *et al.*, 2018; Uchida *et al.*, 2008; Pyragas, 1997]. CS is characterized by having all CLEs negative and at least one Lyapunov exponent positive [Zhou & Lai, 1998]. However, for complex neuronal networks, the study of CS is not well understood due to its intrinsically large number of parameters and degrees of freedom. To address this issue, a simpler technique known as the “auxiliary system” approach has been proposed [Abarbanel *et al.*, 1996]. This approach tracks the possible trajectories for the driven system with a unique driver signal, independently of initial conditions in the driven subsystem.

The auxiliary system approach calculates the distance between the real system and the auxiliary trajectory, which indicates how far apart the initial conditions may be in the phase space. This approach is used to detect the Complete Synchronization process in a driven system (or subsystem).

The application of signals in chaotic systems has been utilized as a means of controlling chaos, with the goal of stabilizing unstable periodic orbits through small perturbations to the system. Examples include the OGY (Ott, Grebogi and Yorke) method [Ott *et al.*, 1990; Lai & Grebogi, 1993] and the Pyragas control method, which employs continuous perturbations [Pyragas, 1992; Pyragas & Tamaševičius, 1993; Pyragas, 2006]. These methods are typically applied after acquiring sufficient knowledge of the system dynamics over a suitable period of time.

In recent years, the ideas presented by Pecora in his seminal work on Chaos Synchronization [Pecora & Carroll, 1990] have found significant applications in encryption [Keuninckx *et al.*, 2017; Moon *et al.*, 2021] and cryptography [Antonik *et al.*, 2018; Aliabadi *et al.*, 2022]. The concerns of current research on factors affecting CS involve the analysis of how synchronization begins in a dynamical system, recent studies show results of the microscopic dynamics at the attractor level [Lahav *et al.*, 2018]. Specifically, it has been found that sparse areas of the attractor with lower expansion rates initiate the synchronization process, which can lead to complete synchronization if enough of these local converging effects accumulate along the trajectory [Lahav *et al.*, 2022]. We anticipate that this characteristic could be enhanced in systems with higher dimensionality, as seen in complex networks — a novel aspect proposed in our study.

In other aspects, works have explored the use of spiking neural networks (SNNs) as a means to increase computational capability while replicating the biological neurons’ behavior, resulting in higher unitary complexity [Subbulakshmi Radhakrishnan *et al.*, 2021; Tavanaei *et al.*, 2019]. SNNs have been proposed as a bridge between machine learning processing capabilities and accurate emulation of biological dynamics in neuroscience [Ghosh-Dastidar & Adeli, 2009; Maass, 1997]. To create such networks, individual neurons with periodic or chaotic dynamics are necessary. However, in the chaotic scenario, the network may be sensitive to initial conditions, leading to different outcomes depending on the starting point [Ott, 2002]. Here, we explore different configurations to control the sensitivity to initial conditions in a network that is forced by another subnetwork, similar to a topology commonly found in feed-forward networks [Haykin, 1999].

Our focus in this study is to investigate the impact of network structure on chaos synchronization rather than the intricacy of a realistic model for neuron simulation. To this end, we employ a two-dimensional map capable of simulating bursting, spiking, and resting patterns [Rulkov, 2001]. To quantify synchronization, we define a metric that captures the time for a pair of trajectories to be close enough to be considered synchronized. We use this metric to analyze the temporal evolution and parameter spaces. We also explore four important algorithms for network construction and find that each network topology is associated with a specific

set of parameters for which synchronization with the master is achieved.

## 2. The Model

The system consists of two networks externally linked via a directed connection, in a master-slave setup. Our analysis relies on the time evolution of the slave network, which is cared as the subsystem of interest. We explore a parameter related to individual chaotic dynamics and significant coupling configurations.

Both, analyses and network simulations have been implemented utilizing the Julia programming language [Bezanson *et al.*, 2017], which provides an efficient environment for fast numerical simulations and scientific computation.

### 2.1. Rulkov map

For the simulation of the individual dynamics, we use the Rulkov map [Rulkov, 2001], which is composed of two algebraic equations

$$x(n+1) = \frac{\alpha}{1+x(n)^2} + y(n), \quad (1a)$$

$$y(n+1) = y(n) - \sigma x(n) - \beta, \quad (1b)$$

where parameters  $\sigma$  and  $\beta$  determine the recovery rate of the slow variable  $y(n)$ , (we use here  $\sigma = \beta = 0.005$ ). The fast variable  $x(n)$  simulates the membrane voltage of a neuron and is modulated by the slow variable  $y(n)$ .

The variable  $x(n)$  exhibits a range of behaviors, transitioning from simple spikes to chaotic bursts by varying the parameter  $\alpha$ . Figure 1 illustrates the distinct characteristics of the  $x(n)$  and  $y(n)$  dynamics. Panel (a) shows regular spiking behavior, panel (b) depicts triangular bursting, and panel (c) exhibits irregular bursting. The transition from periodic to chaotic dynamics in the Rulkov model is noteworthy. The map falls into a stable point, known as the resting phase, for  $\alpha < 2.0$ . However, for  $\alpha > 4.5$ , it becomes difficult to differentiate between firing and quiescent dynamics, which are not related to neural dynamics and therefore not considered.

Rulkov's analysis of the Rulkov map [Rulkov, 2001] describes the intermittency between irregular bursts and the quiescent period. He treats  $y(n)$  as a parameter with respect to  $x(n)$  and analyzes the fast variable as a one-dimensional map. In the

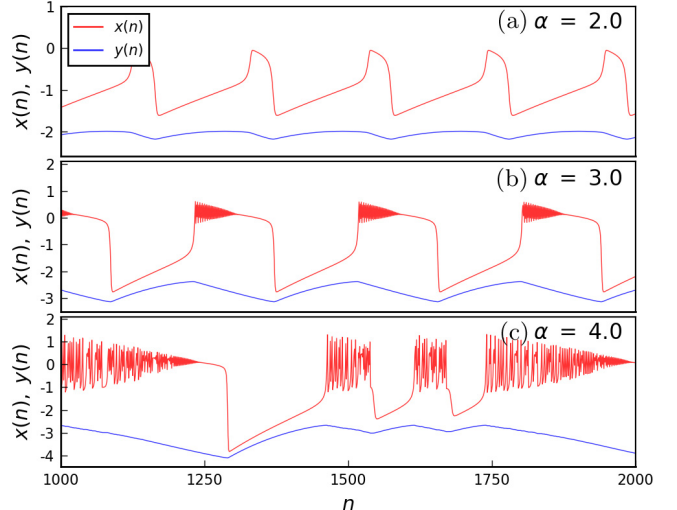


Fig. 1. Individual dynamics of a Rulkov map, for parameters: (a)  $\alpha = 2.0$ , (b)  $\alpha = 3.0$  and (c)  $\alpha = 4.0$ ; and for every case  $\sigma = \beta = 0.005$ . We illustrate the effect of the nonlinear parameter  $\alpha$  on the bursting behavior of a neuron.

bifurcation diagram, there is a region where three fixed points coexist, one stable and two unstable. A burst begins when the parameter  $y(n)$  removes the map from this stable configuration and stops when  $y(n)$  returns, resulting in a quasi-period. When  $\alpha$  is small, there is only one stable fixed point — which incurs the resting dynamics.

The two-dimensional map used in our study serves as a simplified model that captures essential aspects of more complex models, while also allowing for fast and efficient computation. Nevertheless, we anticipate that our paper will provide an initial framework and direction for more rigorous investigations in the future.

### 2.2. The master-slave network structure

The system consists of two networks, namely the slave (driven) network and the master (driver) network, both comprising the same number of neurons  $N$ . The master network does not receive any external signal, while the slave network is subjected to the influence of the master network, as shown in Fig. 2.

Each neuron in the network receives inputs from other neurons within the same network. In addition, the neurons in the slave network receive the mean-field of the master network as an additional driver. The dynamics of each neuron is

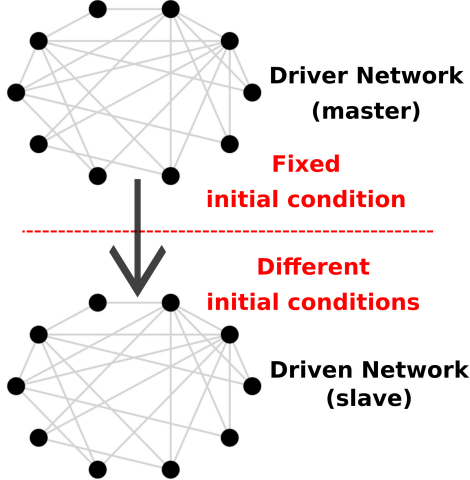


Fig. 2. The master-slave networks structure. To make the analysis in terms of CS, the signal sent by the master must be the same regardless of different initial conditions in the slave, where we compare trajectories of different initial conditions in the slave given one single random initial condition in the master.

described by the following set of equations:

$$x_{k,i}(n+1) = \frac{\alpha}{1 + x_{k,i}^2(n)} + y_{k,i}(n) + I_{k,i}(n) + E_{k,i}(n), \quad (2a)$$

$$y_{k,i}(n+1) = y_{k,i}(n) - \sigma x_{k,i}(n) - \beta, \quad (2b)$$

where  $x_{k,i}$  and  $y_{k,i}$  are the fast and slow variables of the  $i$ th neuron in the subnetwork  $k$  ( $k = m$  for the master network, and  $k = s$  for the slave network). The individual dynamics time scale of the neurons is characterized by the parameters  $\sigma = \beta = 0.005$ . The parameter  $\alpha$  takes values in the range  $\alpha = 2.1$  to  $\alpha = 3.0$  so we analyze the triangular bursting dynamics of Rulkov neurons.

It is important to note that in order to analyze the system in terms of CS, the signal sent by the master network must be the same regardless of different initial conditions in the slave network. Therefore, given this requirement, here we are interested to find at least one pair of trajectories that become the same (completely synchronizes) after some chaotic transient.

The inputs  $I_{k,i}(n)$  and  $E(n)$  are the coupling terms with respect to the  $i$ th neuron. The first is due to neurons from the same subnetwork  $k$ ,

$$I_{k,i}(n) = \frac{\varepsilon_{\text{int}}}{N} \sum_{j=1}^N A_{i,j} x_{k,j}(n), \quad (3)$$

where  $\varepsilon_{\text{int}}$  is the internal coupling strength and  $A_{i,j}$  is the internal adjacency matrix. They carry the information on how the subnetworks are internally connected. To keep the model simple, we employ just unweighted graphs; if the neuron  $i$  receives a connection from neuron  $j$  then  $A_{i,j} = 1$ , or  $A_{i,j} = 0$  otherwise. Furthermore, the normalization factor is set equal to the maximum number of connections a neuron in the slave network can receive (in the case of complete connected graphs), it is equal to the number of elements in each layer  $N$ , because  $N - 1$  connections come from neurons in the slave network and one additional connection comes from the master (through the term  $E_{k,i}(n)$ ).

The second input term  $E_{k,i}(n)$  represents external forcing to neurons  $i$  in the network  $k$ , which in our case is the mean-field generated by the master neural network. In this sense, for the master-slave configuration, all neurons in the master network receive no external forcing ( $E_{m,i}(n) = 0$ ), while the only driven neurons are those in the slave network. For these neurons, the external driving term is

$$E_{s,i}(n) = \frac{\varepsilon_{\text{ext}}}{N} \sum_{i=1}^N x_{m,i}(n), \quad (4)$$

where  $\varepsilon_{\text{ext}}$  is the external coupling strength, and the driver signal sent from the master to the slave is proportional to the master network mean-field, this way all neurons receive the same forcing for simplicity.

To analyze the dependence on internal topology, we need to explore a parametric space of networks with a large number of degrees of freedom. However, the computational power required might be high, so we limit ourselves to studying small networks (with ten nodes). Although small, such networks are sufficient to test various graph models.

We choose four representative graphs to build the subnetworks, and we describe each of them below:

- (1) **Random regular undirected graph:** This is a very simple graph generator, where each node randomly connects to exactly  $k$  neighbors via undirected connections. The adjacency matrix is therefore symmetric. We use a fixed  $k = 3$  for our experiments.
- (2) **Complete graph:** Also known as Global Connected Lattices, this graph is used as a limit case for densely connected networks. It is an undirected regular graph with degree  $N - 1$ , so

- every node is connected to all of its neighbors from the same layer.
- (3) **Random regular directed graph:** Each node in this graph has the same out-degree  $k_{\text{out}}$ , which means it has  $k_{\text{out}}$  links departing from it to random neighbors. We set  $k_{\text{out}} = 3$  for our experiments. This generator is the limit case of sparse networks and leads to interesting results, such as parameters with rapid convergence to the synchronized state.
- (4) **Barabási–Albert model:** To highlight the different outcomes of each internal topology, we consider a random graph constructed using the Barabási–Albert model [Barabási & Albert, 1999]. This is a scale-free network built starting from a small graph (we use a cycle graph with three nodes). Each new node is randomly connected to three existing ones. Therefore, the mean degree ends up slightly higher than three, and the main difference from the random regular topology is the presence of hubs with higher degree  $k$  than the average.

To conduct our analysis, we have kept certain aspects of the network architecture generators fixed, but not necessarily the exact connection matrix, as the construction algorithm may involve random factors. Additionally, we varied the couplings  $\varepsilon_{\text{int}}$  and  $\varepsilon_{\text{ext}}$  because our objective was to highlight the potential of network structures for studying chaos synchronization.

We believe that our approach may provide insights for future implementations of more suitable frameworks, which could potentially address other aspects of network architecture. This could lead to improved and refined methodologies for investigating chaos synchronization in network systems.

### 3. Quantifier for Synchronization of Trajectories Over the Same Forcing Signal

In the master-slave system, inspired by the approach introduced in [Pecora & Carroll, 1990], we explore the time evolution of various initial conditions in the slave subsystem while constraining the master subsystem to a specific initial condition. This technique, referred to as “the auxiliary system approach” in Chaos Synchronization setups [Abarbanel *et al.*, 1996], enables us to examine the response of the slave subsystem to a fixed input signal.

We note that the auxiliary system approach only analyzes the time evolution of a pair of initial conditions, so it does not measure the statistical behavior of an ensemble of possible trajectories, one suggestion would be to use modified versions of statistical synchronization factors [Xu *et al.*, 2017; Wu *et al.*, 2018a; Wu *et al.*, 2018b], what could be computationally demanding for high-dimensional neural system simulations. For this first work, we use only the auxiliary system as a more reliable approach due to its standard and simple way to quantify CS (commonly used in low-dimensional systems) rather than modified measures of synchronization between oscillators in networks.

To quantify the differences between trajectories initiated from different initial conditions, we utilize the Euclidean distance in phase space within the subspace of the slave system  $s$ , denoted as

$$\|x_s(n) - x_s^*(n)\| = \left( \sum_{i=1}^N \{[x_{s,i}(n) - x_{s,i}^*(n)]^2 + [y_{s,i}(n) - y_{s,i}^*(n)]^2\} \right)^{1/2}, \quad (5)$$

where  $x_{s,i}^*(n)$  and  $y_{s,i}^*(n)$  are auxiliaries variables, which involves creating multiple instances of the auxiliary system that receive the same input from the master but possess distinct random initial conditions.

The synchronization of trajectories is indicated by

$$\|x_s(n) - x_s^*(n)\| \rightarrow 0,$$

if we observe it for several initial conditions, we observe that the synchronization occurs regardless of the chosen initial condition. This outcome is determined by a combination of parameters, in our case the more significant ones are  $\alpha$ ,  $\varepsilon_{\text{int}}$ , and  $\varepsilon_{\text{ext}}$ . In the next section, we show that synchronization can occur even if the autonomous system is chaotic, resulting in what is known as Chaos Synchronization (CS).

To detect the occurrence of synchronization of trajectories, we use a quantifier that captures the degree of trajectory synchronization. This is achieved by counting the number of times the distance between two different trajectories in phase space is smaller than a predefined threshold value  $\epsilon$ . If this count exceeds a certain value, we can infer

that synchronization has taken place. Using the Heaviside function, we define the quantifier  $F$ :

$$F = \frac{1}{n_f} \sum_{n=1}^{n_f} \Theta(\epsilon - \|x_s(n) - x_s^*(n)\|), \quad (6)$$

where  $n_f$  is the total of time steps considered, we do not discard the transient period of time as this measure is used to also estimate the duration of chaotic transients.

The quantifier  $F$  provides a measure of how quickly two trajectories converge over synchronization due to a common driver signal. For rapid synchronization processes  $F \approx 1$ , systems for different initial conditions result in different trajectories  $F = 0$ . In this work, we consider the indicator of CS for any observed value of  $F$  greater than zero for some pair of simulated trajectories.

#### 4. CS in Master-Slave Setup of Rulkov Maps

Firstly, we present the results for a master-slave system of two coupled Rulkov neurons, with the equations of motion being the same as in Eq. (2), considering  $i = N = 1$  and

$$I_{m,i}(n) = I_{s,i}(n) = 0, \quad (7a)$$

$$E_{s,i}(n) = \varepsilon_{\text{ext}} x_{m,i}(n). \quad (7b)$$

The difference from the original case [Eq. (2)] is the absence of internal connections, there is no  $\varepsilon_{\text{int}}$  as well as any dependence on internal topology. The only coupling is the directed connections via Rulkov's fast variable from the master to the slave. Therefore in this simple system, the only parameters of interest are  $\alpha$  and  $\varepsilon_{\text{ext}}$ .

We use the quantifier  $F$  described in Sec. 3 and compare it with traditional quantifiers of dependence on initial conditions, which are the maximum Lyapunov and maximum conditional Lyapunov exponents, this result is shown in Fig. 3, where the coupling is held fixed in a value of  $\varepsilon_{\text{ext}} = 0.1$  and the parameter  $\alpha$  is varied.

For small values of  $\alpha$  the maximum Lyapunov exponent  $\lambda_{\max}$  of the autonomous system is equal to zero, so the Rulkov map is not chaotic. In an intermediary region, between  $\alpha = 2.6$  and  $\alpha = 3.1$ , the  $\lambda_{\max}$  sign depends highly on  $\alpha$ , as shown in Fig. 3(b), this region corresponds to the transition from periodic to chaotic dynamics. Finally, in a

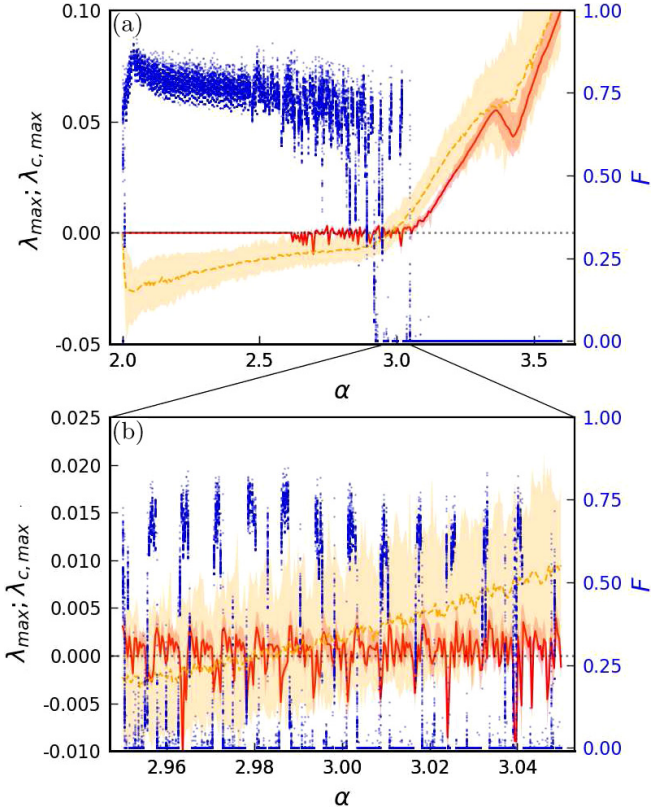


Fig. 3. Maximum Lyapunov exponents for the autonomous and for the driven systems and quantifier  $F$  [Eq. (6)] as a function of  $\alpha$ . The curves correspond to the maximum Lyapunov exponent of the autonomous Rulkov map (solid red) and the maximum conditional Lyapunov exponent for the master-slave system of two Rulkov neurons (dashed orange)  $\varepsilon_{\text{ext}} = 0.1$ , the blue dots correspond to computations of  $F$  using random pairs of initial conditions. In total we proceed to 256 trials, the lines indicate the mean values while the shaded areas indicate the minimums and maximums over the trials. (a) A wider range of parameters, (b) an amplification in the transition from synchronized to unsynchronized dynamics.

region for greater values of  $\alpha$  the maximum Lyapunov exponent is always greater than zero so arbitrary near-initial conditions diverge. The maximum conditional Lyapunov exponent  $\lambda_{c,\max}$  has a similar performance of  $\lambda_{\max}$  for either small or great values of  $\alpha$ . In the transition region to chaotic dynamics both  $\lambda_{c,\max}$  and  $\lambda_{\max}$  are near zero with considerable error bars. So  $\lambda_{c,\max}$  has dependence on initial condition than  $\lambda_{\max}$ .

The quantifier  $F$  can detect long transients, when it is neither near 0 or 1, just as the dependence on pairs of initial conditions for the occurrence of chaos synchronization if an ensemble of pairs is considered. In Fig. 3, some pairs of initial conditions converge quickly while others may have longer

chaotic transients, this reveals a different type of dependence on initial conditions than commonly used to distinguish periodic from chaotic motion. In this scenario, the convergence rate of a pair of different initial conditions is highly dependent on where such conditions have been selected and not on local properties. Therefore, as the maximum Lyapunov exponent can only quantify the convergence rate of nearby initial conditions, the capability of distant ones to converge is only observed by  $F$ .

The main loss from the simple master-slave coupling of two Rulkov maps is the impossible change of internal coupling architecture or exploring the  $(\varepsilon_{\text{int}}, \varepsilon_{\text{ext}})$  plane, as we are going to show rich structures that stress the role of plasticity for the stability control. Therefore, the next section is dedicated to the exploration of networks of Rulkov maps. We show how chaotic transient duration and the global stability of complex networks might be highly dependent on the connections' structure.

## 5. CS in Master-Slave Networks

The impact of the parameter  $\alpha$  on the occurrence of CS is typically a loss of synchronization as  $\alpha$  increases. However, there is an exception in the transition region where the convergence of pairs of initial conditions is not solely dependent on the value of  $\alpha$ . This section focuses on exploring different coupling architectures, and we demonstrate that the same qualitative behavior observed for the

parameter  $\alpha$  is also present when the parameters  $\varepsilon_{\text{ext}}$  and  $\varepsilon_{\text{int}}$  are varied.

The dependence on connections for the occurrence of CS is an important trait for networks where the change in connection weights is an expected mechanism because CS could suppress perturbations, thus inducing stability in a driven network. In the brain and in machine learning, learning is achieved through network plasticity [Hebb, 2002; Hopfield, 1982; Markram *et al.*, 1997; Silveira *et al.*, 2021], which consists of a rule to update connection weights in order to optimize a desired behavior.

The effect of changes in connection weights in our system for its stabilization or destabilization is illustrated in Fig. 4, where we show how an applied perturbation can be either suppressed or persist for different coupling strengths in a network. The perturbation is applied by a time span of 1000 time steps and amplitude similar to the Rulkov neuron, being sufficiently strong to mismatch the trajectories and to remove them from near the attractor. After its application, some disturbances last for only short periods of time, others are not quickly suppressed or may persist indefinitely, as shown by the maximum cutoff simulation time of  $10^6$  time steps.

The quantifier  $F$  is designed to capture the dependence of synchronization on the nonfixed parameters  $\varepsilon_{\text{int}}$  and  $\varepsilon_{\text{ext}}$ , thus it can be written as  $F = F(\varepsilon_{\text{int}}, \varepsilon_{\text{ext}})$ . However, we should note that the value of  $F$  also depends on the graph model used to construct the layers, as it affects the overall

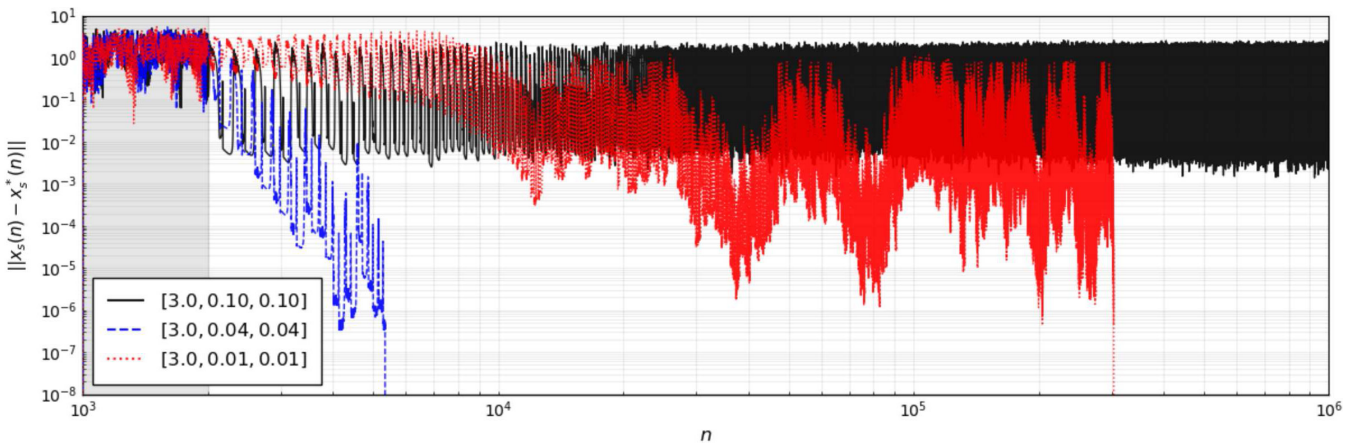


Fig. 4. Progression of disturbances when a perturbation is applied in the slave network, the perturbation is applied by 1000 time steps (indicated by the gray area). Here is shown a case using the Barabási-Albert model and parameters in the form  $[\alpha = 3.0, \varepsilon_{\text{int}}, \varepsilon_{\text{ext}}]$ , for fixed nonlinear parameter  $\alpha$  and three different coupling strengths: in dotted red for small internal coupling, in dashed blue for intermediary coupling and in solid black for high value of coupling. We show that the stability of the driven system can be determined by the intensity of coupling between neurons, the black curve exemplifies the nonoccurrence of CS, the red a long chaotic transient prior to the synchronization, and in blue a quick stabilization after the perturbation.

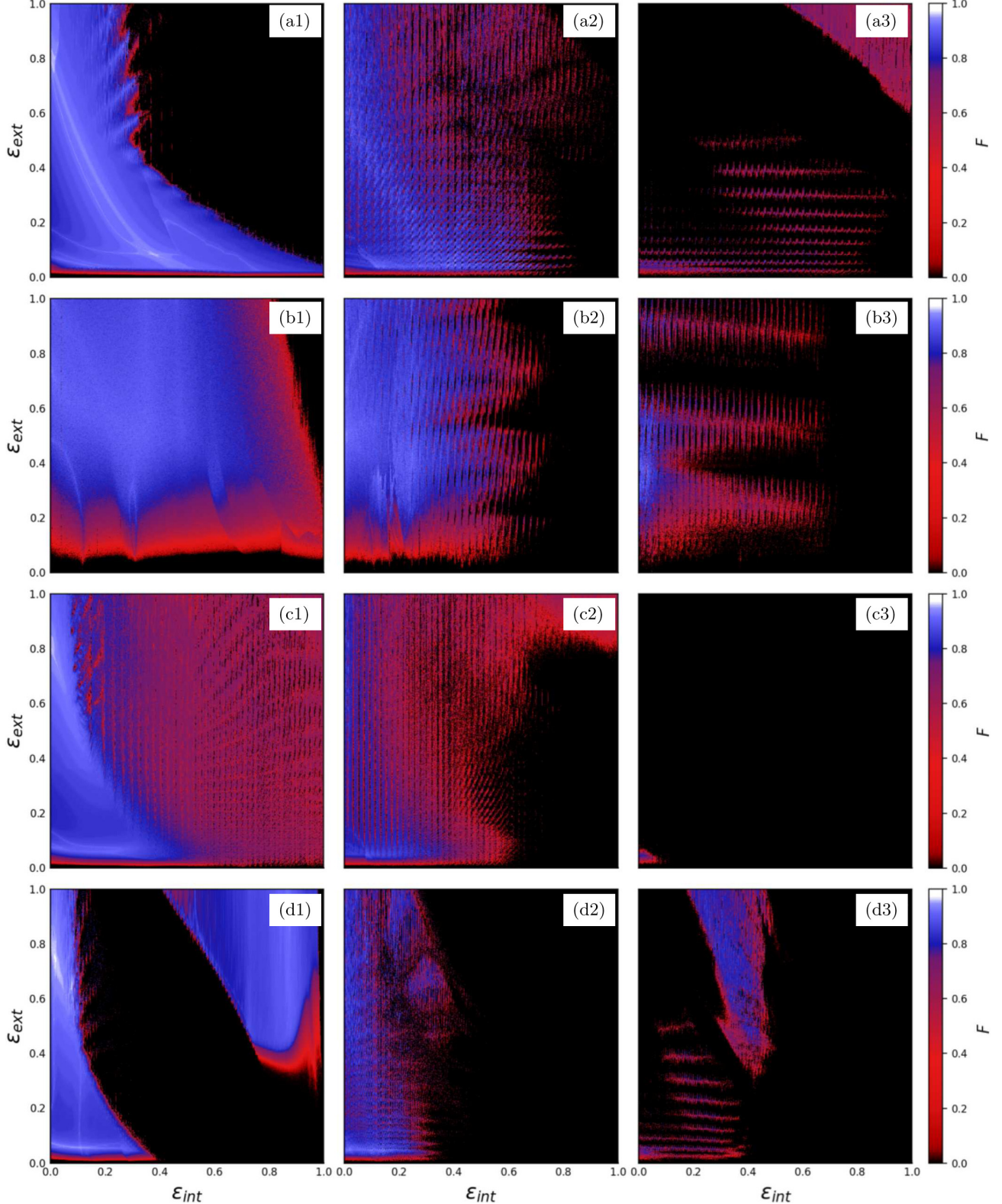


Fig. 5. Parametric space for different networks and nonlinear parameter  $\alpha$ , as a function of coupling parameters. The network architectures employed are (a) random directed, (b) random undirected, (c) Barabási–Albert and (d) complete graph, whereas the nonlinear parameters are (.1)  $\alpha = 2.1$ , (.2)  $\alpha = 2.5$  and (.3)  $\alpha = 3.0$ . The panels emphasize not only the stability's dependence on the nonlinear parameter but also the coupling scheme used to build the networks. We assess the sensibility with coupling architecture and coupling strength by the variety of patterns generated using  $F$  for networks built using different algorithms. Each network's specificity is described in the text.

equation of motion.  $F$  measures the percentage of simulation time during which the driven system remains synchronized, taking into account the possible presence of long chaotic transients.

In Fig. 5, we show the diagrams in the couplings parametric space for the four network architectures previously presented and three representative values of  $\alpha$ . The panels emphasize the dependence on the nonlinear parameter  $\alpha$  (the individual dynamics) and the graph generator (the collective structure) for the occurrence of CS. While the axis emphasizes the dependence on internal and external coupling strengths,  $\varepsilon_{\text{int}}$  and  $\varepsilon_{\text{ext}}$  respectively.

In the panels of Fig. 5, regions where  $F(\varepsilon_{\text{int}}, \varepsilon_{\text{ext}}) \rightarrow 1$  correspond to combinations of parameters where the system displays CS, for these parameters the dynamics is stable over applied perturbations in the driven subsystem, and the greater the value of  $F$  the quicker the perturbations are suppressed. For  $F = 0$  the system cannot resume to a single possible trajectory, so CS does not take place. Moreover, the observation of CS rather than periodic behavior is supported by the fact that the values of  $F$ , representing the synchronization measure, are consistently zero in the absence of an external driving force,  $\varepsilon_{\text{ext}} = 0$ .

The main and sturdier structures are similar to *patches*, regions where CS happens, with greater or lesser chaotic transient periods of time. Excluding the borders, *patches* are well defined for each kind of network, meaning each graph generator spans its own pattern in the parameter space of couplings.

The network architecture and the nonlinear parameter are intertwined: for some topologies  $\alpha$  has a starker influence in the overall area where CS takes place. Nevertheless, for every topology analyzed, with  $\alpha$  greater than 3.0 it becomes harder to observe CS for any combination of  $\varepsilon_{\text{int}}$  and  $\varepsilon_{\text{ext}}$ , while for small values (near  $\alpha = 2.0$ ) CS occurs for more combinations of coupling strengths. Thus, the influence of the topology is relevant within this range, in which the Rulkov map displays triangular bursting dynamics.

We notice that the use of couplings near 1 is not ideal and might destroy the expected dynamics for the Rulkov map. For example, we consider the big top-right *patch* in the complete graph [Fig. 5(d)] as an artifact for our procedure, because in it we lose the bursting behavior to a resting one (that is not desirable here). Nonetheless, we cannot predict when this happens, or for what kind of graph it

is expected. For this reason, we maintain the same coupling ranges in every case, keeping in mind this is not a problem from the methodology, but rather from the structural dynamical complexity of the proposed system.

The *patches* borders are undefined and fluctuate in  $F$  in a random fashion, which reflects the variability of the initial conditions for each parameter combination used. As previously mentioned, in the transition region from periodic to chaotic dynamics, the duration of chaotic transients depends heavily on the pair of initial conditions analyzed. We hypothesize that there is a probability of observing CS due to the multitude of available transient trajectories. Different rates of CS observation are necessary to determine the time evolution when convergence rates are significant to establish the occurrence of CS, which we explore in the next section.

Within the parametric regions where CS occurs, other patterns can be observed, characterized by a rapid convergence of trajectories over time, forming regions that resemble *veins*. However, these patterns are difficult to track, as they are highly dependent on the network as a whole and the settling process. When producing several diagrams, the *veins* are never exactly the same when the initial conditions for each parameter set are not fixed, in contrast to the *patches* with CS, which mostly depend on the internal topology of the network. This observation suggests that local convergence rates are crucial for the time when CS is detected, but if it will occur depends only on the coupling architecture and bifurcation parameter.

The best case to visualize the curves of rapid CS is for random directed networks and small nonlinear parameter  $\alpha$ . In other words, sparse graphs with near periodic individual dynamics [see Fig. 5(a.1)] are the most stable setups, so combinations of parameters for which the convergence rate is elevated are more abundant.

Subsequently, we compute the finite time conditional Lyapunov spectrum of a network for several different initial conditions. We aim to corroborate the assumption that CS depends mostly on momentary strong convergence rates in the driven system.

## 6. Finite Time Lyapunov Exponents Correlation with Chaos Synchronization

The master-slave scheme we employ imposes the same forcing signal for all initial conditions in

the slave network, regardless of their location in the state space. Therefore, our intention is not to restrict the analysis to neighboring initial conditions. In this sense, the quantifier  $F$  does not capture local properties as it does not necessarily compare neighboring initial conditions, unlike traditional tools such as Lyapunov exponents. In this section, we make a comparison between the quantifier we proposed and traditional tools to study dynamical systems to assess their differences.

We computed the conditional Lyapunov exponents for the driven system using a fixed set of initial conditions in the driver. In future works, more advanced tools such as the Covariant Lyapunov Vectors [Ginelli *et al.*, 2007] or the Master Stability Function [Arenas *et al.*, 2008; Pecora & Carroll, 1998] could be employed to analyze, respectively, the directions of expansion or contraction associated with the exponents and their dependence on topology.

However, computing Lyapunov exponents can be computationally demanding, especially for systems with a high degree of freedom, which can become even worse when exploring the various parameters that define a complex network. Therefore, we restricted our analysis to the main diagonal of the above diagrams, only analyzing the dependence on coupling strengths by setting  $\varepsilon = \varepsilon_{\text{int}} = \varepsilon_{\text{ext}}$ .

The method we use to compute the Lyapunov spectrum is called H2, which is described in [Geist *et al.*, 1990]. It involves adding the signal sent by the master in each iteration and the evaluation of the growth rates in each direction of a  $2N$ -dimensional parallelepiped, where  $N$  is the number of neurons in the subnetwork. The method also requires the specification of a relaxation time and a subsequent range over which the computation is effectively carried out.

In Fig. 6, we show the Lyapunov spectrum of the driven network in a simple master-slave setting of random directed networks with  $\alpha = 2.1$  and  $N = 10$  neurons. We used a relaxation period of 10 000 time steps and a computation range of 200 time steps. We note that we do not compute the usual Lyapunov exponents, but rather finite-time ones. The computation is carried out over approximately one characteristic time period of the bursts, followed by a relaxation period that is equal to the total time window used to analyze CS in the parametric space [see Fig. 5(a.1)].

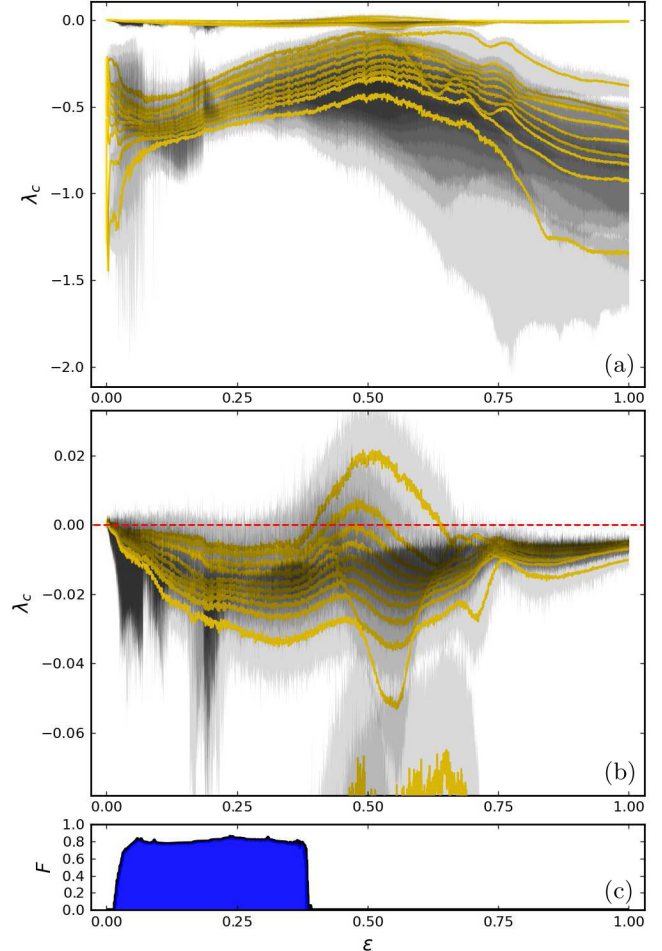


Fig. 6. Finite time conditional Lyapunov spectrum and CS quantifier  $F$  for a sparse network, randomly directed with 10 neurons, as a function of the overall coupling strength. We reduce the number of parameters to analyze the imposing relation  $\varepsilon_{\text{int}} = \varepsilon_{\text{ext}} = \varepsilon$ . The panels present: (a) the complete spectrum, (b) the amplification of the region near  $\lambda_c = 0.0$  (where the largest ten exponents accumulate), and (c) the values of  $F$  as a function of  $\varepsilon$ . We show results for a random regularly directed network to build the master and the slave networks, the computation is undertaken for 200 time steps after a transient of 10 000 time steps, thus it enables a proper comparison with the result presented in Fig. 5(a.1). In panels (a) and (b) the yellow curves are the mean values of Lyapunov exponents spectrum of 50 trials, while in black are the respective uncertainties for each exponent.

Comparing the diagonal of Fig. 5(a.1) with the conditional Lyapunov exponents shown in Fig. 6, we can establish a correlation between the CS measurements obtained through  $F$  and the dependence on neighboring initial conditions, as shown in panel (c). The regions where  $F$  indicates CS begins where there is at least one mean positive Conditional Lyapunov exponent. In contrast, small coupling regions

with no positive exponents exhibit CS, indicating that the information is provided by  $F$  and  $\lambda_{c,\max}$ . In this sense, the advantage of  $F$  over  $\lambda_{c,\max}$  is its minimal computational demand.

However, for high coupling values, all the finite time conditional Lyapunov exponents are lesser than zero, so although  $F$  indicates the trajectories are not the same, there is local convergence in their small neighborhood. We cannot infer the reason it occurs but the results indicate this parametric region is associated with stability but not complete synchronization, for instance, CS with lag or multiple attracting trajectories.

As a last issue, we note the considerable uncertainty associated with the most prominent Conditional Lyapunov exponents, indicating that some regions of the attractor exhibit higher convergence rates of nearby initial conditions than others. Therefore, the time required for Chaos Synchronization to occur is highly dependent on the initial condition's location set in the driven network, while its occurrence is highly dependent on parameter definitions such as the network's coupling architecture.

The duration of chaotic transients, which depends on the initial state, suggests that disturbances may evolve in different ways and require different amounts of time to be suppressed if CS occurs. The dependence on the coupling architecture indicates that network plasticity could play a role in stabilizing the network, ensuring that external perturbations have no effect on the system's dynamics.

## 7. Conclusions

In this study, we have demonstrated the occurrence of Chaos Synchronization (CS) in a master-slave configuration of networks of Rulkov Map oscillators. We have used a simple quantifier to measure the time when two trajectories stay close to each other, which combined with Lyapunov exponents analysis reveals properties of the high-dimensional driven dynamical system during the transition from a chaotic transient to complete synchronization.

Our results indicate that for small nonlinear parameter values, CS occurs in the master-slave configuration of two Rulkov Maps. However, for higher values of the nonlinear parameter, intricate dynamics occurs during the transition to chaotic dynamics, where there is a sensitivity to initial

conditions for the duration of the chaotic transient and to the nonlinear parameter value for the occurrence of CS.

The sensitivity, with a nonmonotonic dependence on the parameters, of CS highlights the significant role played by the coupling architecture in complex networks. However, the presence of unique parameter sets for each network generator where CS becomes conceivable indicates that the network stability is not excessively sensitive to minor modifications in a few connections. This reliance on coupling strengths and network topology implies that connection plasticity potentially acts as an agent for ensuring dynamical stability in driven complex networks, such as the brain, thereby facilitating learning and memory formation.

In future works, we intend to statistically analyze the evolution of several initial conditions in the transient dynamics, test plasticity rules, and study the features a signal must have to suppress chaos in complex networks of oscillators. These findings will enhance our understanding of the intricate dynamics of CS in complex networks, which have important implications for a wide range of scientific and engineering fields.

## Declaration of Competing Interest

The authors declare that they have no known competing financial interests or personal relationships that could have appeared to influence the work reported in this paper.

## Acknowledgments

We wish to acknowledge the *DynamicalSystem.jl* project [Datseris, 2018] that helped not only in the Lyapunov analysis but also with other useful quantifiers and predefined dynamical systems for occasional trials.

This work was supported by the following Brazilian research agencies: *Conselho Nacional de Desenvolvimento Científico e Tecnológico* (CNPq), Grants Nos. 308621/2019-0, 305189/2022-0, 403120/2021-7, 301019/2019-3 and 308441/2021-4; *Coordenação de Aperfeiçoamento de Pessoal de Nível Superior* (CAPES) through projects Nos. 88881.143103/2017-01 and 88887.833325/2023-00; and *Fundação de Amparo à Pesquisa do Estado de São Paulo* (FAPESP) through Grant No. 2022/04251-7.

## References

- Abarbanel, H., Rulkov, N. & Sushchik, M. [1996] “Generalized synchronization of chaos: The auxiliary system approach,” *Phys. Rev. E* **53**, 4528–4535.
- Aliabadi, F., Majidi, M.-H. & Khorashadizadeh, S. [2022] “Chaos synchronization using adaptive quantum neural networks and its application in secure communication and cryptography,” *Neur. Comput. Appl.* **34**, 6521–6533.
- Antonik, P., Gulina, M., Pauwels, J. & Massar, S. [2018] “Using a reservoir computer to learn chaotic attractors, with applications to chaos synchronization and cryptography,” *Phys. Rev. E* **98**, 012215.
- Arenas, A., Díaz-Guilera, A., Kurths, J., Moreno, Y. & Zhou, C. [2008] “Synchronization in complex networks,” *Phys. Rep.* **469**, 93–153.
- Barabási, A.-L. & Albert, R. [1999] “Emergence of scaling in random networks,” *Science* **286**, 509–512.
- Bezanson, J., Edelman, A., Karpinski, S. & Shah, V. B. [2017] “Julia: A fresh approach to numerical computing,” *SIAM Rev.* **59**, 65–98.
- Boccaletti, S., Kurths, J., Osipov, G., Valladares, D. & Zhou, C. [2002] “The synchronization of chaotic systems,” *Phys. Rep.* **366**, 1–101.
- Datseris, G. [2018] “Dynamicalsystems.jl: A julia software library for chaos and nonlinear dynamics,” *J. Open Source Softw.* **3**, 598.
- Eroglu, D., Lamb, J. & Pereira, T. [2017] “Synchronization of chaos and its applications,” *Contemp. Phys.* **58**, 207–243.
- Geist, K., Parlitz, U. & Lauterborn, W. [1990] “Comparison of different methods for computing Lyapunov exponents,” *Progr. Theoret. Phys.* **83**, 875–893.
- Ghosh-Dastidar, S. & Adeli, H. [2009] “Spiking neural networks,” *Int. J. Neur. Syst.* **19**, 295–308.
- Ginelli, F., Poggi, P., Turchi, A., Chaté, H., Livi, R. & Politi, A. [2007] “Characterizing dynamics with covariant Lyapunov vectors,” *Phys. Rev. Lett.* **99**, 130601.
- Haykin, S. [1999] *Neural Networks: A Comprehensive Foundation*, International edition (Prentice Hall).
- Hebb, D. [2002] *The Organization of Behavior: A Neuropsychological Theory* (Taylor & Francis).
- Hopfield, J. J. [1982] “Neural networks and physical systems with emergent collective computational abilities,” *Proc. Natl. Acad. Sci. USA* **79**, 2554–2558.
- Keuninckx, L., Soriano, M. C., Fischer, I., Mirasso, C. R., Nguimdo, R. M. & Van der Sande, G. [2017] “Encryption key distribution via chaos synchronization,” *Scient. Rep.* **7**, 43428.
- Lahav, N., Sendiña Nadal, I., Hens, C., Kshetrim, B., Barzel, B., Cohen, R. & Boccaletti, S. [2018] “Synchronization of chaotic systems: A microscopic description,” *Phys. Rev. E* **98**, 052204.
- Lahav, N., Sendiña-Nadal, I., Hens, C., Kshetrim, B., Barzel, B., Cohen, R. & Boccaletti, S. [2022] “Topological synchronization of chaotic systems,” *Scient. Rep.* **12**, 1–10.
- Lai, Y.-C. & Grebogi, C. [1993] “Synchronization of chaotic trajectories using control,” *Phys. Rev. E* **47**, 2357–2360.
- Lerescu, A., Constandache, N., Oancea, S. & Grosu, I. [2004] “Collection of master-slave synchronized chaotic systems,” *Chaos Solit. Fract.* **22**, 599–604.
- Maass, W. [1997] “Networks of spiking neurons: The third generation of neural network models,” *Neural Netw.* **10**, 1659–1671.
- Maritan, A. & Banavar, J. R. [1994] “Chaos, noise, and synchronization,” *Phys. Rev. Lett.* **72**, 1451–1454.
- Markram, H., Lübke, J., Frotscher, M. & Sakmann, B. [1997] “Regulation of synaptic efficacy by coincidence of postsynaptic APs and EPSPs,” *Science* **275**, 213–215.
- Moon, S., Baik, J.-J. & Seo, J. M. [2021] “Chaos synchronization in generalized Lorenz systems and an application to image encryption,” *Commun. Nonlin. Sci. Numer. Simul.* **96**, 105708.
- Ott, E., Grebogi, C. & Yorke, J. A. [1990] “Controlling chaos,” *Phys. Rev. Lett.* **64**, 1196–1199.
- Ott, E. [2002] *Chaos in Dynamical Systems*, 2nd edition (Cambridge University Press).
- Pecora, L. M. & Carroll, T. L. [1990] “Synchronization in chaotic systems,” *Phys. Rev. Lett.* **64**, 821–824.
- Pecora, L. M. & Carroll, T. L. [1991] “Driving systems with chaotic signals,” *Phys. Rev. A* **44**, 2374–2383.
- Pecora, L. M. & Carroll, T. L. [1998] “Master stability functions for synchronized coupled systems,” *Phys. Rev. Lett.* **80**, 2109–2112.
- Pyragas, K. [1992] “Continuous control of chaos by self-controlling feedback,” *Phys. Lett. A* **170**, 421–428.
- Pyragas, K. & Tamaševičius, A. [1993] “Experimental control of chaos by delayed self-controlling feedback,” *Phys. Lett. A* **180**, 99–102.
- Pyragas, K. [1997] “Conditional Lyapunov exponents from time series,” *Phys. Rev. E* **56**, 5183–5188.
- Pyragas, K. [2006] “Delayed feedback control of chaos,” *Philos. Trans. Roy. Soc. A: Math. Phys. Engin. Sci.* **364**, 2309–2334.
- Rulkov, N. F. [2001] “Regularization of synchronized chaotic bursts,” *Behav. Brain Sci.* **86**, 183–186.
- Silveira, J. A. P., Protachevicz, P. R., Viana, R. L. & Batista, A. M. [2021] “Effects of burst-timing-dependent plasticity on synchronous behaviour in neuronal network,” *Neurocomputing* **436**, 126–135.
- Soriano, D. C., dos Santos, O. V., Suyama, R., Fazanaro, F. I. & Attux, R. [2018] “Conditional Lyapunov exponents and transfer entropy in coupled bursting neurons under excitation and coupling mismatch,” *Commun. Nonlin. Sci. Numer. Simul.* **56**, 419–433.

- Subbulakshmi Radhakrishnan, S., Sebastian, A., Oberoi, A., Das, S. & Das, S. [2021] “A biomimetic neural encoder for spiking neural network,” *Nature Commun.* **12**, 1–10.
- Tavanaei, A., Ghodrati, M., Kheradpisheh, S. R., Masquelier, T. & Maida, A. [2019] “Deep learning in spiking neural networks,” *Neural Netw.* **111**, 47–63.
- Uchida, A., Yoshimura, K., Davis, P., Yoshimori, S. & Roy, R. [2008] “Local conditional Lyapunov exponent characterization of consistency of dynamical response of the driven Lorenz system,” *Phys. Rev. E* **78**, 036203.
- Wu, F., Zhou, P., Alsaedi, A., Hayat, T. & Ma, J. [2018a] “Synchronization dependence on initial setting of chaotic systems without equilibria,” *Chaos Solit. Fract.* **110**, 124–132.
- Wu, F.-Q., Ma, J. & Ren, G.-D. [2018b] “Synchronization stability between initial-dependent oscillators with periodical and chaotic oscillation,” *J. Zhejiang Univ.-Sci. A* **19**, 889–903.
- Xu, Y., Jia, Y., Ma, J., Alsaedi, A. & Ahmad, B. [2017] “Synchronization between neurons coupled by memristor,” *Chaos Solit. Fract.* **104**, 435–442.
- Zhou, C. & Lai, C.-H. [1998] “Synchronization with positive conditional Lyapunov exponents,” *Phys. Rev. E* **58**, 5188–5191.